

www.acsanm.org Forum Article

# Ionic-Liquid-Modified Nanoparticles as Potential Mucus Modulators for Nasal Drug Delivery

Mary E. VanLandingham, Rebekah A. Heintz, Chathuri S. Kariyawasam, Donovan S. Darlington, Claylee M. Chism, Sara X. Edgecomb, Angela Roberts, Jorden Marzette, Nicholas C. Fitzkee, and Eden E. L. Tanner\*



Cite This: https://doi.org/10.1021/acsanm.3c03807



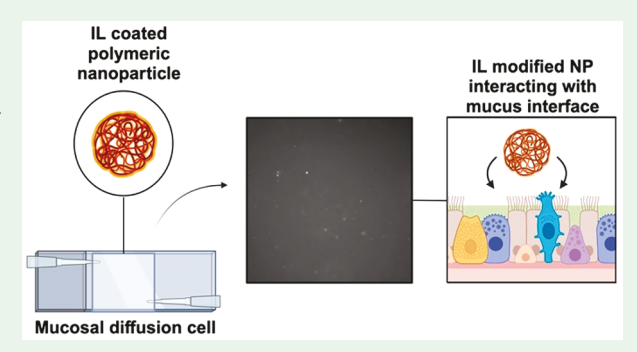
ACCESS

Metrics & More

Article Recommendations

Supporting Information

ABSTRACT: Mucosal barriers are a natural defense system for preventing the entry of foreign objects into the body; however, they pose obstacles for effective drug delivery. Coated polymer nanoparticles (NPs) have been shown to possess improved rates of diffusion across mucus compared to their uncoated, or bare, counterparts. Choline carboxylic acid-based ionic liquids (ILs) are highly tunable and show high biocompatibility and mucus modulation properties, making them an ideal choice for the improvement of NP diffusion through mucosal barriers. This study aimed to investigate whether the use of choline-based ILs has a positive effect on the dispersibility of poly(lactic-co-glycolic acid) (PLGA), poly(ethylene glycol) methyl ether-block-poly(lactide-co-glycolide) (PEG-PLGA),



and poly(ethylene glycol)—poly(lactic acid) (PEG—PLA) NPs through nasal mucus by using a multiple particle tracking method. The samples, according to the IL used, showed altered rates of diffusion in both aqueous and mucosal environments. The use of CA2HE 1:1 with PEG—PLGA NPs slowed NP diffusion, while the use of the same IL increased diffusion for PEG—PLA. Additionally, UV—vis spectroscopy was used to identify the possible formation of complexes between the mucin polymer and NPs. Circular dichroism (CD) spectroscopy was used to analyze any potential changes in the secondary structure of mucin as a result of the introduction of polymeric NPs. It was demonstrated that the use of an IL can stabilize the interactions between polymer NPs and mucin polymers. Isothermal titration calorimetry was used to obtain quantitative measurement of the binding energies between NPs and mucus and serves to confirm the results obtained from CD spectroscopy. Last, an ex vivo porcine nasal mucosa model was used to explore their use in a nasal delivery context, disclosing a possible connection between the use of zwitterionic transport materials and more effective drug delivery. This research demonstrates the potential of choline carboxylic acid-based ILs to control the transport behavior of polymer NPs for intranasal drug delivery.

KEYWORDS: drug delivery, ionic liquids, nanoparticles, mucin, mucus, diffusion

#### 1. INTRODUCTION

Within the field of drug delivery, delivery through the nasal passages is of special interest due to its noninvasive nature as well as the ability to transport both locally and potentially through the blood-brain barrier (BBB). There are several issues to overcome in order to successfully use the nasal passages for drug transport. First, mucus serves as a 5–15  $\mu$ m barrier to prevent foreign substances from easily entering the body, including therapeutic drugs introduced to the body. 1-3 Furthermore, the mucociliary clearance mechanism clears mucus out every 15-20 min and carries the filtered substances into the gastrointestinal tract.<sup>4</sup> Another potential issue is the enzymatic degradation of external substances. One of the main components of mucus, mucin, is a highly glycosylated protein with oligosaccharide side chains and sialic acid groups, which yield an overall negatively charged molecule. 2,5 At a neutral pH, the hydrophobic regions of mucin are buried within folds, with salt bridges between positively and negatively charged amino acids providing a stabilizing effect. Due to the very limited time frame, the unwillingness to harbor chemicals alien to the body, and the overwhelmingly negative charge of the mucus, it is necessary to overcome this barrier between the pharmaceuticals and the bodily environment to effectively deliver drugs.

Polymeric nanoparticles (NPs) are a promising choice for the transportation of therapeutic materials. They can

Special Issue: Women in Nano

Received: August 15, 2023 Revised: October 12, 2023 Accepted: October 12, 2023



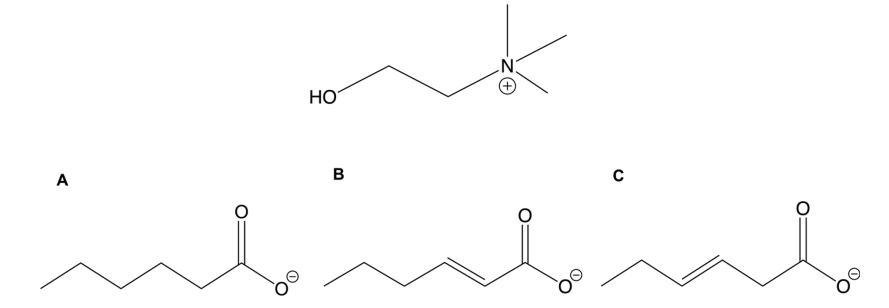


Figure 1. Structures of a choline cation and hexanoic (A), 2-hexenoic (B), and 3-hexenoic (C) anions.

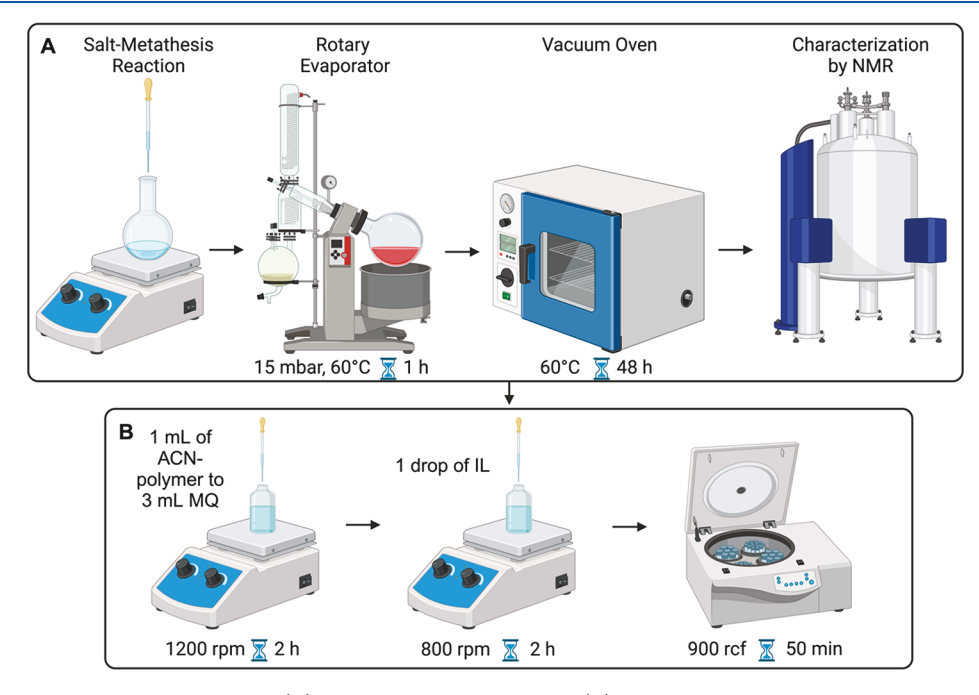


Figure 2. Schematic illustrating the IL synthesis (A) and NP assembly methods (B).

biodegrade into parts that the body can process (unlike metal NPs or other particulates), can be tuned to slowly release the cargo over an extended period of time, and show the ability to penetrate further into the mucosal barrier compared to free drug molecules. 5,7,8 It is mostly thought that electrostatic interactions are the primary means of interaction between the mucin and NPs. 3,5,9-11 Poly(lactic-co-glycolic acid) (PLGA) particles are promising candidates for polymeric NPs because of their biocompatibility, biodegradability, and FDA approval. Conjugation of a poly(ethylene glycol) (PEG) chain onto the PLGA chain via an ester linkage yields the other two polymers used in this project: PEG-PLGA and closely related PEG-PLA [poly(lactic) acid, which omits the glycolic coblock polymer in PLGA]. There are a few benefits to PEGylated particles. PEGylated particles have different diffusion values compared to unmodified polymers, and PEG provides some shielding effects to the internal (hydrophobic) polymer, which increases the overall hydrophilicity of the particles. 1,3,11,12 Further modification is also possible for these particles with the use of ionic liquids (ILs). ILs are bulky salts that are liquid at room temperature. They are also capable of stabilizing the NPs that they are capping. Many different types of ILs exist, but choline-based ILs (Figure 1) are of particular interest because of their high biocompatibility and mucus-modulating properties, which may allow for improved uptake of pharmaceutical

molecules. Choline, in particular, is beneficial because it is capable of shielding the polymer NPs from the negatively charged mucin, as well as reducing the viscosity of the mucus without significantly changing its structure. Herein we use a host of tools to investigate the movement of IL NPs through artificial mucus, possible interactions between the mucin molecule and NPs [UV–vis spectroscopy, circular dichroism (CD) spectroscopy, and isothermal titration calorimetry (ITC)], and finally an ex vivo porcine nasal mucosa model to assess whether transport through mucus is mirrored in the mucosal tissue.

### 2. EXPERIMENTAL SECTION

**2.1. Materials.** Resomer RG 504 H, poly(D,L-lactide-co-glycolide) acid 50:50, poly(ethylene glycol) methyl ether-block-poly(L-lactide-co-glycolide) with molecular weights of 5–25 kDa and with a lactic acid to glycolic acid ratio of 50:50, poly(ethylene glycol)-block-poly(lactic acid) diblock copolymer with molecular weights of 1–5 kDa, choline bicarbonate ( $\sim$ 80% in H<sub>2</sub>O), hexanoic acid ( $\geq$ 99% solution), trans-2-hexenoic acid ( $\geq$ 98%), trans-3-hexenoic acid ( $\geq$ 98%), Rhodamine B ( $\geq$ 95% solution), acetonitrile (ACN), mucin from porcine stomach type II were all purchased from Sigma-Aldrich (St. Louis, MO). Artificial nasal mucus fluid was obtained from Biochemazone (Waterloo, Ontario, Canada). A 10× phosphate-buffered saline (PBS) solution was obtained from Research Products International (Mt. Prospect, IL). Fresh pig heads were obtained from Smokehouse

Meats (Pontotoc, MS) and used immediately. Any water used was filtered through a Millipore-Sigma ultrapure water system and had 18  $M\Omega$ -cm resistivity.

- **2.2. Synthesis and Characterization of ILs.** The synthesis of ILs begins with the addition of 5 g of a choline cation to a round-bottomed flask containing hexanoic acid at a 1:1 or 1:2 molar ratio (Figure 2A). Together, they reacted in a salt metathesis reaction to form the IL. Using a rotary evaporator, the solution was dried at 15 mbar, for 1 h, at 60 °C. Additionally, a vacuum oven was also used to dry out the IL for 48 h at 60 °C. A Karl Fisher coulometric titrator was used afterward to determine the water content. The successful synthesis of the IL was confirmed with <sup>1</sup>H NMR spectroscopy (see the SI for full characterization).
- 2.3. Assembly of NPs. The assembly of polymeric NPs begins with the addition of 3 mL of purified water and a magnetic stir bar to a 20 mL scintillation vial (Figure 2B). If PEG-PLGA is used, 10 mL of purified water should be used instead. In a separate vial, we combined the polymer and ACN until homogeneous using a vortex mixer. For PLGA, we used a 1 mg/mL ratio. For PEG-PLGA, we used 1.2 mg of polymer and 101  $\mu$ L of ACN. For PEG-PLA, we used a 1.2 mg/mL ratio. To create fluorescent particles, a Rhodamine B stock solution was measured out to equal 4% of the weight of the polymer and added to the polymer-ACN mixture before vortexing, except in the case of the PEG-PLGA NPs assembled for the ex vivo experiments, where Rhodamine B was added to the aqueous phase. Using a 1 mL Pasteur pipet, the mixture was added dropwise to the water. The solution was allowed to spin at 1200 rpm for 3 h. If no capping was required, the solution was purified using centrifugation at 980 rcf for 50 min at 4 °C with 30K molecular weight cutoff filters. This was done to separate out the NPs from excess dye and other unnecessary components in the solution. The size and surface charge of the NPs were measured with a Malvern Zetasizer DLS instrument. The parameters were as follows: DTS0012 cell; PLGA material; water dispersant; run in triplicate. The equilibrium time was reduced to 10 s. Furthermore, the general-purpose model was selected for the analysis model, and the fluorescence filter was used due to the presence of Rhodamine B. The same settings were used for measurement of the  $\zeta$  potential.
- 2.3.1. Modification of NPs with Choline-Based ILs. After spinning the bare particles for 3 h at 1200 rpm, a drop of IL was added to the center of the solution vortex and spun at 800 rpm for an additional 2 h. Centrifugation followed afterward at 980 rcf for 50 min at 4  $^{\circ}$ C.
- 2.4. Collection and Analysis of Diffusion Videos. In order to obtain the diffusivity constants, the use of an Eclipse Ts2-FL inverted microscope was required to analyze samples at 40× magnification. The settings used were epifluorescence with a tetramethylrhodamine isothiocyanate filter. It was necessary to build diffusion cells in which the samples could be observed diffusing through the chosen medium. The cells were composed of a microscope slide, with a square Parafilm border enclosed on top with a coverslip. Two 10  $\mu$ L pipet tips were embedded within the Parafilm and positioned across from one another. NIS-Elements was used to capture short videos (n = 12) per sample to analyze the diffusion rates. Then, using the Python package trackpy, it was possible to extrapolate the values for diffusivity. The program tracks both the particles and frames. By doing this, the program is able to determine how fast the particle is traveling, and from that, it extrapolates the diffusion coefficients that were provided in the output. The parameters for the Python box were size = 15, memory = 10, min mass = 20, max size = 7, and max ecc = 0.5. The size parameter could be increased by 2 up to size = 21 if particle tracking failed. Additionally, studies comparing the diffusions of PLGA NPs within mucus, water, and mucin solutions, as well as a time study over the course of 4 h, were performed, and can be found within the SL
- **2.5.** UV–Vis Analysis of NP–Mucus Interactions. The interactions between mucin and the polymer NPs were investigated by using an Agilent UV–Vis-NIR spectrophotometer along with the Cary WinUV software program. The region scanned was from 200 to 800 nm. Rhodamine B-dyed PLGA, PEG–PLGA, and PEG–PLA NPs, both bare and capped with CA2HE 1:1, were added to 130  $\mu$ L

- of mucus solutions by increasing the amounts of increments until a total of 1 mL had been added. Measurements were taken after each increment was introduced to the solution.
- **2.6.** CD Analysis of NP–Mucin Interactions. CD spectroscopy was used to identify whether any changes were made to the secondary structure of porcine gastric mucin (PGM) with the addition of polymeric NPs. The region ranging from 200 to 260 nm was scanned using a Jasco J-1000 spectropolarimeter. A quartz cuvette with a path length of 1 mm was used. All three polymeric NPs and their CA2HE 1:1 capped counterparts were analyzed along with PGM with this technique. Furthermore, a concentration study was performed for the CA2HE 1:1 PEG–PLGA NPs (see the Supporting Information, SI). The concentration of the mucin solution was 2 mg/mL mucin polymer in Milli-Q water. To start, 20  $\mu$ L of NPs was added to the initial mucin solution, and further additions of 20  $\mu$ L were added until 100  $\mu$ L total was in the solution. Measurements were taken after each addition of the NPs.
- 2.7. Isothermal Titration Calorimetry. ITC measurements were performed on a Microcal VP-ITC instrument (GE Healthcare). All of the mucin and NP solutions were made in Milli-Q water to ensure a buffer match. Mucin (3  $\mu$ M) in the ITC syringe was titrated into NP dispersions with various concentrations in the ITC cell to achieve isotherms with a sigmoidal transition. A typical experiment used 3  $\mu$ M mucin and 200-300 nM particles. Both protein and NP samples were degassed for 10 min before the experiments. A total of 28 injections, each with 10  $\mu$ L in volume, or 35 injections, each with 8  $\mu$ L volume, were typically used, with an equilibration time of 6 min between injections. The cell was continuously stirred at 480 rpm, and the cell temperature was maintained at 25 °C during each experiment. For each experiment, baseline corrections for the raw thermograms were performed using NITPIC,  $^{14,15}$  and the thermodynamic parameters N, K, and  $\Delta H$  were fitted using CHASM. The heat of the final injection was used as the baseline in each experiment. Control experiments were performed to determine the heat of dilution of the NPs and protein into the buffer; in all cases, the dilution heats were less than 10% of the observed enthalpy, and no further corrections were made. All ITC experiments were performed in triplicate (or more) using independently prepared replicate samples, and the uncertainties in N, K, and  $\Delta H$  are reported as the standard error of the mean from these replicates.
- **2.8. Ex Vivo Permeability Studies.** For the ex vivo permeability studies, a modified procedure of Chatzitaki et al. was used. Fresh pig heads were obtained from a local slaughterhouse (Smokehouse Meats, Pontotoc, MS). The nasal mucosa tissue was immediately excised and washed with 1× PBS prewarmed to 37 °C. After filling the receptor chambers to the top with prewarmed 1× PBS, the tissue was then mounted on Franz diffusion cells so that the mucosal side of the tissue faced the donor chamber. Conductivity testing was then performed to assess the tissue integrity. Afterward, the diffusion cells were placed on a stir plate set to 100 rpm in an incubator set to 37  $^{\circ}\text{C}$  to mimic in vivo conditions. A total of 100  $\mu$ L of each Rhodamine B-tagged IL NP sample was placed in the donor chamber using Parafilm and aluminum foil to seal and protect the compartment from light. Nasal mucosa treated with only 1× PBS under the same conditions was used as a control. At time periods of 15, 30, 45, 60, 90, 120, 150, 180, 210, and 240 min, 500  $\mu$ L was taken from the receptor chamber and replaced with an equal amount of prewarmed 1× PBS. Approximate concentrations of the IL NP samples found at each time point were obtained by using a plate reader, measuring fluorescence at 570/590 nm (ex/em).

## 3. RESULTS AND DISCUSSION

**3.1.** IL Synthesis and Identity Confirmation. Synthesis of the ILs was achieved through a 1:1 or 1:2 salt metathesis reaction between the choline cation and the hexanoic or hexenoic anion, where the choline was added dropwise and allowed to mix and react for 24 h. The removal of any excess water occurred over time in the rotary evaporator (at 60 °C and 10 mbar) and vacuum oven. <sup>1</sup>H NMR analyses were used

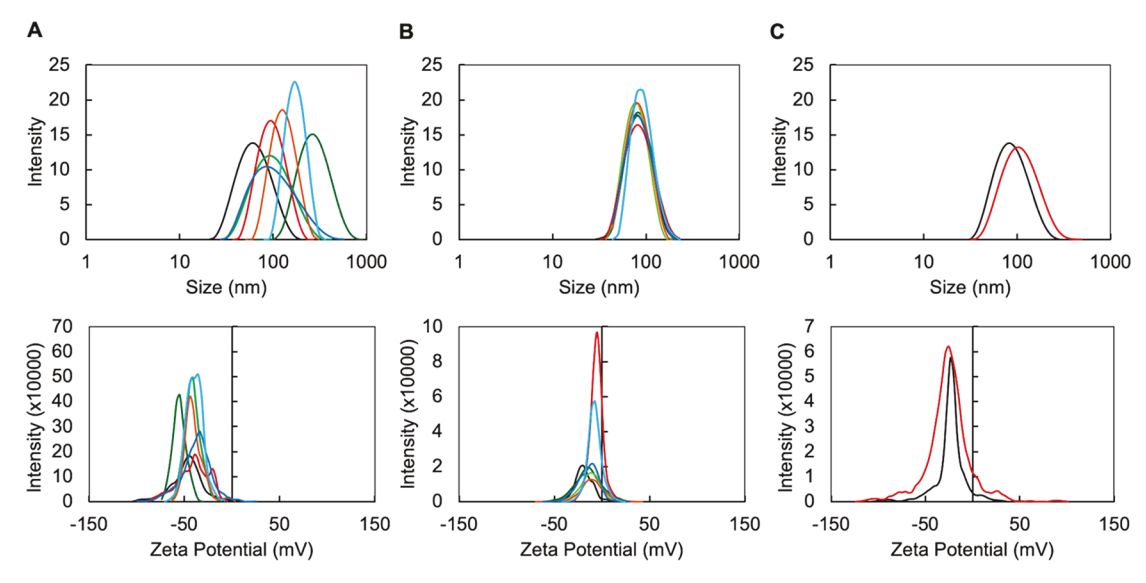
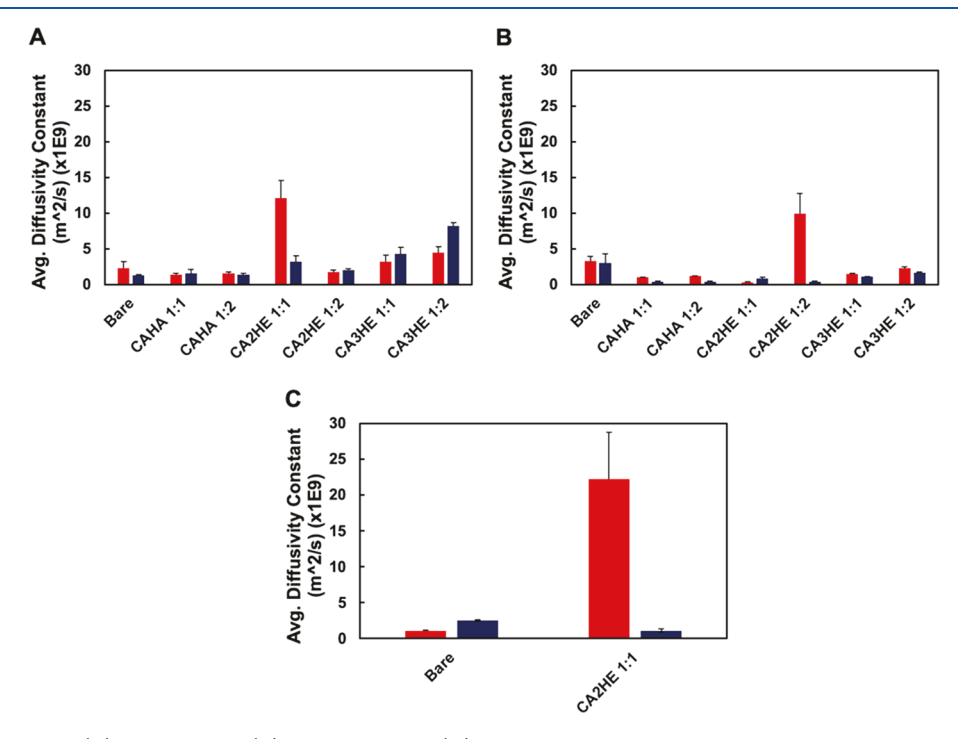


Figure 3. Size and ζ potential of PLGA NPs (A), PEG-PLGA (B), and PEG-PLA (C): bare, black; CAHA 1:1, dark green; CAHA 1:2, light green; CA2HE 1:1, red; CA2HE 1:2, brown; CA3HE 1:1, blue; CA3HE 1:2, light blue.



**Figure 4.** Diffusion of PLGA (A), PEG-PLGA (B), and PEG-PLA (C) NPs: mucus, red; water, blue. n = 12, reported as mean + standard error of the mean.

to confirm the identity of the IL (see the SI). Further information about the synthetic yield and purity of the ILs used can be seen in the SI.

**3.2.** NP Modification Effects on the Size and Surface Potential. The NPs were assembled as described in Section 2.3. A Malvern Zetasizer was used to conduct dynamic light scattering (DLS) to measure the size distribution and surface potential of the NPs. For the bare PLGA NPs, the average size was  $59.1 \pm 1.1$  nm, and the  $\zeta$  potential was  $-48 \pm 1.6$  mV (Figure 3). The addition of a choline-based IL, on average, shifted the size distribution by at least 40 nm. The  $\zeta$  potential shifted as well to become slightly more negative, reflecting the successful capping of the NPs. As seen in Figure 3, for the bare PEG-PLGA NPs, the average size was  $79.9 \pm 3.4$  nm and the

 $\zeta$  potential was  $-18.2 \pm 1.8$  mV. The addition of a choline-based IL, on average, did not shift the size distribution more than 5 nm, with the exception of CA3HE 1:2, which shifted the size by 9 nm. The  $\zeta$  potential was shifted to become more positive. This is of particular interest as the sialic acid groups in mucin are negatively charged and thus will react more strongly with NPs with a more positive surface charge. It can be seen that, for bare PEG-PLA NPs, the average size was 79.9 ± 2.6 nm and the  $\zeta$  potential was  $-24.0 \pm 0.5$  mV (Figure 3). The addition of CA2HE 1:1 shifted the size distribution by at least 25 nm. The  $\zeta$  potential did not shift, but the IL is still present within the NPs and thus properly capped. A single drop of IL is not enough to significantly shift the size of either diblock polymer NPs, nor is it enough to shift the  $\zeta$  potential of PEG-

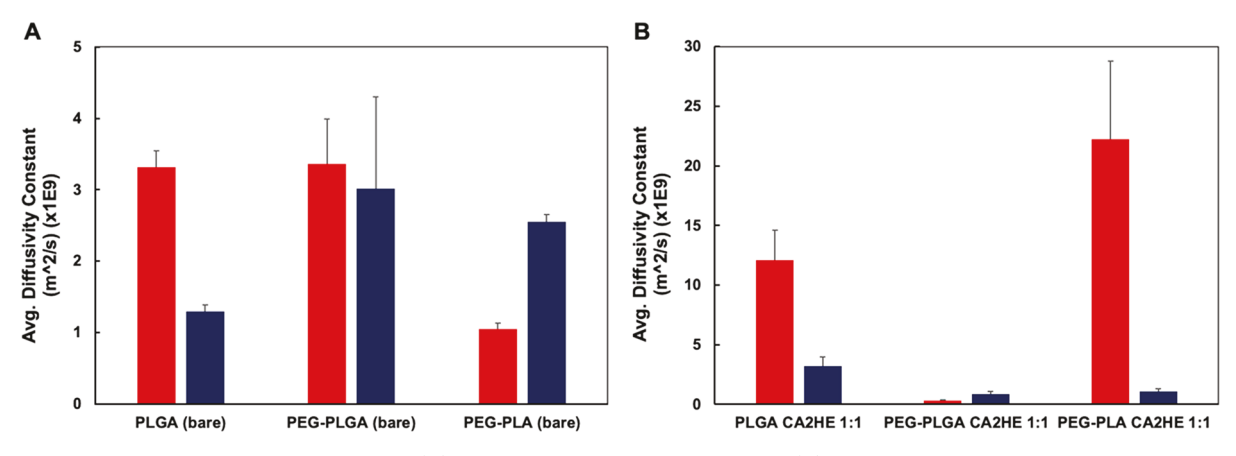


Figure 5. Comparative diffusion plots of bare NPs (A) and NPs modified with CA2HE 1:1 (B): mucus, red; water, blue. n = 12, reported as mean + standard error of the mean.

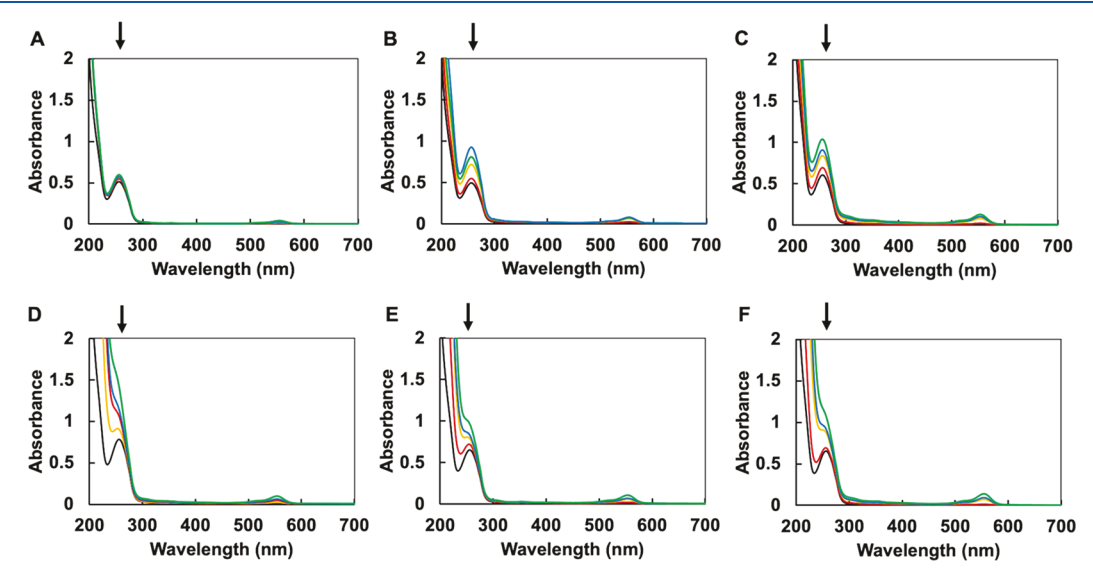


Figure 6. UV—vis spectra for bare PLGA (A), bare PEG—PLGA (B), bare PEG—PLA (C), CA2HE 1:1 PLGA (D), CA2HE 1:1 PEG—PLGA (E), and CA2HE 1:1 PEG—PLA (F): 130  $\mu$ L of mucus, black; 30  $\mu$ L of NPs, red; 110  $\mu$ L of NPs, yellow; 130  $\mu$ L of NPs, blue; 200  $\mu$ L of NPs, green. The black arrows indicate the 260 nm peak produced by the NPs and the mucin.

PLA NPs. This is likely due to the IL filling in the empty space instead of surrounding the particles, as occurs with PLGA NPs.

3.3. Diffusion Rates of Bare and IL-Modified NPs by Optical Tracking. After the assembly, modification, and characterization of the NPs, their diffusion was investigated with the use of custom-made diffusion cells and an optical microscope. Along with the bare uncapped sample, the six different anion combinations for the ILs were also investigated. As seen in Figure 4A, in all PLGA samples except the IL coated with CA2HE 1:1, the average diffusion constant decreased in mucus, and thus the particles moved slower than when solvated in water. Tracking bare particles in water proved difficult, which could be due to their hydrophobic nature, which prevented clear videos from being easily obtained. It is shown that, for the PEG-PLGA NPs, in all cases but CA2HE 1:2, the average diffusion rate in mucus decreased compared to that in the control (Figure 4B). This makes sense because all IL-capped NPs had a more positive surface charge than their bare counterparts. More positively charged particulates will diffuse more slowly through mucus because it has an overall negative charge due to its sialic acid groups. The CA2HE 1:2capped NPs are the exception to this trend. This indicates that

the diffusion seems to be controlled by interactions between the mucin and IL (or NP). The presence of the double bond in 2-hexenoic acid may be causing the anion backbone to become more rigid, reducing the possible interactions between the ILcoated NPs and mucin. In water, the diffusion rate became slower for every IL. It is possible that PEG is acting like a lubricant for the bare PEG-PLGA particles, and so when IL is added, there are comparatively more interactions taking place between the water molecules and the charged surfaces of the NPs, which slows them down. The CA2HE 1:1-coated NPs, in fact, had the slowest diffusion rate for all samples across all polymers and ILs tested, which was measured to be 3.42  $\pm$  $0.59 \times 10^{-10}$  m<sup>2</sup>/s (Figure 4B). It can be seen that the diffusion of IL-capped PEG-PLA is faster than that of bare PEG-PLA in a mucus solution. Similar to the CA2HE 1:2 PEG-PLGA NPs, the addition of the IL has an effect on the interactions between the mucin polymers and the NPs themselves, allowing for a more rapid diffusion, which is of interest for potentially transporting materials through mucus. On the other hand, in an aqueous solution, the diffusion of bare PEG-PLA NPs is the faster value between the two, at  $2.55 \pm 0.10 \times 10^{-9}$  m<sup>2</sup>/s, however, still much slower than that

with the addition of the IL in mucus. The faster diffusion of the uncapped NPs in water is likely due to the hydrophilicity of the PEG portion of the diblock polymer, as seen in the PEG–PLGA as well. The time study and mucin diffusion data can be seen in the SI.

3.3.1. Comparison between Polymer NPs. In mucus, bare PLGA and bare PEG-PLGA had similar rates of diffusion, within the range of  $3.0 \pm 0.5 \times 10^{-9}$  m<sup>2</sup>/s, which can be seen in Figure 5A. Comparatively, uncapped PEG-PLA diffusion in mucus was significantly slower than either bare PLGA or PEG-PLGA diffusion; however, in water a diffusion closer to that of bare PEG-PLGA was yielded, both of which were faster than that of bare PLGA. A two-tailed Student's t test was performed on the data for the uncapped PEG-PLGA and PEG-PLA NPs, which showed no statistical difference (p >0.5). This could be due to the influence of the hydrophilic PEG in the PEGylated samples in contrast to the solely hydrophobic PLGA NPs. Modification with CA2HE 1:1 yielded different results, however. The rate of diffusion of the modified PLGA NPs in water was faster than those of the capped PEG-PLGA and PEG-PLA particles. The latter two appeared similar enough to analyze with another two-tailed Student's t test, but the results showed no statistical similarities. On the other hand, it is seen that the rate of diffusion of CA2HE 1:1-capped PEG-PLA NPs increased along with that of CA2HE 1:1-capped PLGA NPs, but because both polymer NPs yielded similar size and more negative  $\zeta$ potentials compared to CA2HE 1:1 PEG-PLGA NPs, such results are somewhat expected (Figure 5B). A two-tailed Student's t test was used to compare the mucus and aqueous diffusion constants of each polymer. Only the bare PEG-PLGA NPs had statistically similar diffusions in water and

3.4. Investigation of NP-Mucus Complexes by UV-**Vis.** The relationship between the NPs and mucosal proteins was monitored for the possible formation of complexes using UV-vis spectroscopy (Figure 6). After the addition of 130  $\mu$ L of mucus to 2 mL of Milli-Q water, Rhodamine B-loaded NPs were added in increasing increments to the quartz cuvette. Scans were recorded after each addition until 1 mL of total NPs was added or the peak around 280 nm showed no appreciable changes. The spectra revealed the presence of two major peaks in both the bare and capped samples, for all polymers. Three components exist in the solutions that will produce peaks in a UV-vis spectrum. The first is the Rhodamine B dye, which is the source of the sloped peak around 560 nm, due to its excitation and emission wavelengths being 546 and 570 nm, respectively. All polymer NPs produce peaks around 260 nm, contributing to the second peak. This was confirmed by a separate study of dye-loaded NPs without the presence of mucin. Finally, PGM produces an absorbance peak at 258 nm, another contributor to the second peak. As increasing amounts of NPs were added to the solution, the overall absorbance of both peaks increased. This hyperchromicity suggests the formation of complexes between the NPs and proteins in the mucus. When capped NPs were used, the absorbance of the 260 nm peak increased at a faster rate. This pattern was seen in all three polymers.

**3.5. Secondary Structural Changes in NP–Mucin Interactions.** To further develop our understanding of the interactions between mucin and NPs, CD spectroscopy was used to monitor the secondary structure of PGM as bare and IL-modified polymeric NPs were added to the system (Figure

7). A 2 mg/mL solution of PGM powder in Milli-Q deionized water was measured first, and then 20  $\mu$ L of bare, dye-loaded

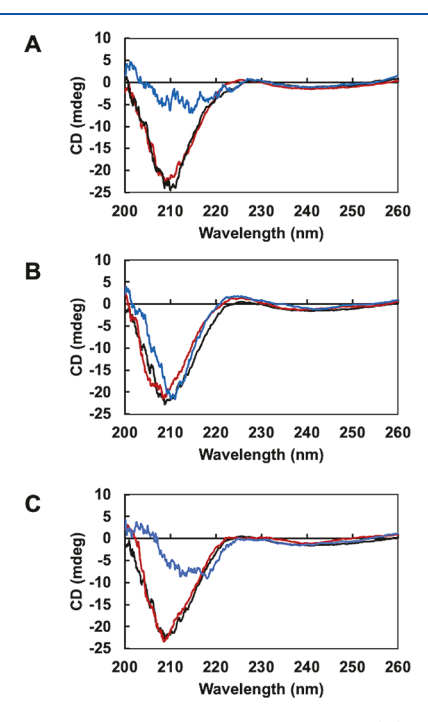


Figure 7. CD spectra for bare and capped PLGA (A), PEG-PLGA (B), and PEG-PLA (C) particles: PGM, black; bare, red; CA2HE 1:1 NPs, blue.

polymer NPs were added. When the bare PLGA NPs were added, the spectrum did not shift dramatically, meaning the secondary structure of the mucin was not greatly modified by the bare NPs. When CA2HE 1:1-capped PLGA NPs were added to the system, the spectrum shifted more positively and became more uneven in appearance (Figure 7A). This suggests that the interactions with the NPs result in an unfolding of the secondary structure. It is possible that the relatively negative surface charge of the IL-capped NPs caused the change reflected in the spectrum. Using data collected from this work, it is seen that while bare PEG-PLGA NPs interact with the polymers within the mucus in a manner similar to that of PLGA particles, CA2HE 1:1 PEG-PLGA NPs react fairly differently. The diffusion is slower, and the UV-vis spectra reported above support the possibility of NPs forming complexes with the mucin. Using CD spectroscopy, it is seen that the NPs do not greatly change the secondary structure of mucin at lower concentrations (Figure 7B). It is possible that, because the IL-capped samples were more positively charged than the other polymeric candidates, the interactions between them and the mucin were more favorable, preserving the secondary structure of the mucin. Using CD spectroscopy, we see that the curve for bare PEG-PLA NPs closely follows that of mucin, indicating that not many changes are occurring structurally. When the CA2HE 1:1 NPs were added to the solution, however, the spectrum mimics that of the PLGA NPs, and the line becomes more positive and uneven, indicating a change in the secondary structure (Figure 7C). Both PLGA and PEG-PLA IL-modified NPs had faster diffusion in mucus, which likely means the negative surface charges interacting with the negatively charged groups on mucin stimulate an unfolding of the structure. The curve for CA2HE 1:1 PEG-

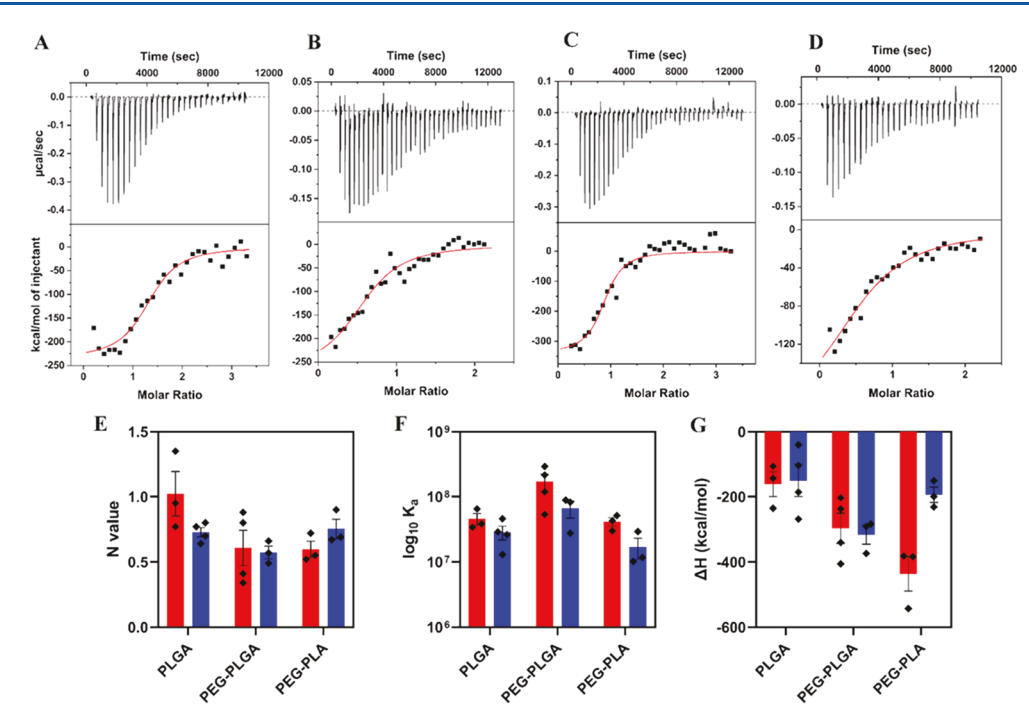


Figure 8. Representative ITC data of mucin titrations to bare PLGA NPs (A), CA2HE 1:1-capped PLGA NPs (B), PEG-PLGA NPs (C), and CA2HE 1:1-capped PEG-PLA NPs (D). The red line indicates the best-fit profile of the integrated heats. ITC parameters stoichiometry (E), binding affinity (F), and binding enthalpy (G) are shown for the bare (red) and CA2HE 1:1-capped (blue) NPs. The error bars represent the standard error of the mean.

PLA is not as positive as that for CA2HE 1:1 PLGA, which could be a result of the PEG diblock, which might help to partially stabilize the structure. It has been shown that mucin's structure is held together with salt bridges, and interactions with acids are capable of breaking these connectors and exposing the hydrophobic regions of the molecule. It is possible that charged species such as capped NPs could also interfere with the salt bridges, thus resulting in the partial unfolding of mucin seen in the CD results.

3.6. Analysis of NP-Mucin Binding Affinities and Enthalpies by ITC. We sought to investigate the binding of mucin to NPs by using ITC. Compared to traditional ITC measurements, where both components are highly purified and homogeneous, the thermograms that we obtained were noisy, reflecting the heterogeneity of the mucin sample. Despite this, reasonable fits could be obtained by increasing the concentration of the NPs, and the fits were consistent (Figure 8). Representative examples are shown in Figure 8, panels A-D, and individual data points are shown in panels E-G to indicate the distribution of observations made from repeated, independent titrations. All of the samples had a stoichiometry of approximately 0.6-1, suggesting that the large mucin molecules cover the NP surfaces and hinder additional binding events. Given that mucin concentrations are estimated from an average molecular size, the distribution of points likely reflects this inhomogeneous distribution. The inhomogeneity of mucin limits the amount of interpretation, but several factors are revealing. First, adding CA2HE 1:1 to bare NPs tends to reduce the binding affinity for PLGA, PEG-PLGA, and PEG-PLA particles (Figure 8F). This trend is consistent with the observed increase in diffusivity when the IL is added. The decrease in affinity likely results from a disruption of weak interactions between the mucin proteins and PLGA/PLA units. The binding enthalpies are more complex: All binding

enthalpies are exothermic, demonstrating the importance of enthalpic interactions such as Coulombic attraction. However, PLGA and PEG-PLGA NPs exhibit a binding affinity similar to that of mucin with or without CA2HE 1:1 (Figure 8G), while the PEG-PLA NPs exhibited comparatively a lower binding affinity to mucin when capped with CA2HE 1:1 IL. At present, it is unclear why the IL makes such a large difference for the PEG-PLA NPs but not the other two systems. The reduction in enthalpy likely contributes to the increase in diffusivity but is apparently not strictly necessary.

These ITC data represent equilibrium thermodynamic binding values. Here, the values of enthalpy and binding affinity appear to correlate with the observations of diffusivity, but diffusion is complex and reflects many different collision events. The measured enthalpy and affinity need not reflect the collisions that occur under steady-state conditions of Brownian motion, and care is required to interpret diffusion in terms of equilibrium binding measurements. Thus, while the correlation between ITC and diffusion is suggestive, ITC is best interpreted as a measure of the equilibrium interaction strength and may not fully represent the kinetics of stochastic collisions.

3.7. Permeability of Bare and Modified NPs in Ex Vivo Conditions. To investigate how the IL-NP samples altered the permeability of the nasal mucosa, ex vivo permeability studies were performed using fresh porcine nasal mucosa and a Franz diffusion cell setup. While these studies will not model nasal transport perfectly because of the lack of active barriers in the ex vivo setup, they allow us to explore the role ILs may play in temporarily altering the permeability of the mucosa. CA2HE 1:1-capped PEG-PLGA samples seemed to permeate the nasal mucosa faster than their bare PEG-PLGA counterparts. Because of the high degree of variability in the tissue, we report here the absolute  $\Delta$  values of the concentration of the bare

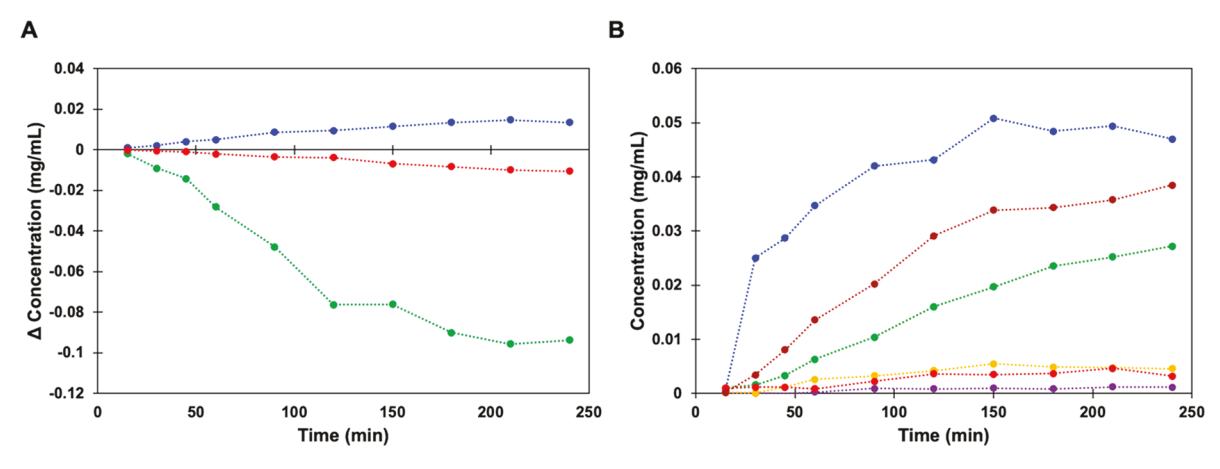


Figure 9. Δ concentration values with respect to time (A). Individually plotted rates of permeation samples 1–3 of CA2HE 1:2 capped with PEG–PLGA NPs and their bare PEG–PLGA counterparts (B): bare S1, purple; bare S2, blue; bare S3, green; CA2HA 1:2 S1, yellow; CA2HA 1:2 S2, black CA;2HA 1:2 S3, red.

PEG-PLGA samples minus the concentration of the CA2HE 1:1-capped PEG-PLGA samples, each analyzed on tissue taken from the same animal. Figure 9A shows that the amount of NPs in the donor chamber decreased for two of the three trials, indicating that 1:1 CA2HE-capped samples permeate the nasal mucosa faster than bare PEG-PLGA. The positive  $\Delta$ value for the outlying trial may be due to differences in tissue integrity, but more studies need to be performed to verify this hypothesis. Alternatively, Figure 9B shows that two of the three samples capped with 1:2 CA2HE displayed permeation rates that were slower than those of their bare PEG-PLGA counterparts. While a small study, the difference in permeation seen with just a change in the anion-to-cation ratio studies still suggests that the differences in diffusion through mucus are correlated with tuned permeability through nasal mucosa. This correlation is further supported in Leal et al.,3 which discusses how successful permeation of epithelia might depend on charge switching or, more specifically, particles with an initial negative charge during diffusion and subsequent positive charge during epithelial permeation.

## 4. CONCLUSIONS

By changing the anion of the choline-based ILs and their ratios, it was possible to obtain different rates of diffusion for the capped NPs. The diffusion coefficients differed between both the IL and polymer used. Using a multiple particle tracking technique, it was determined that CA2HE 1:1 PEG-PLGA NPs yielded the slowest diffusion across all samples, while CA2HE 1:1 PEG-PLA was the overall fastest. Slower diffusion is preferable for local treatment, while faster diffusion can make transport through the BBB more achievable. Furthermore, using UV-vis absorbance spectrometry, it was possible to detect the presence of NP-mucin complexes within a mixture of mucus and NP solution. With the use of a CD spectropolarimeter, the effects of the addition of various polymeric NPs, both bare and capped, were monitored after the addition to a mucin solution. CA2HE 1:1 PEG-PLGA NPs yielded the most stable results of all of the modified NPs. Meanwhile, the ex vivo permeability studies with bare, CA2HE 1:2, and CA2HE 1:2 PEG-PLGA NPs suggest tuned permeability through the nasal mucosa and a correlation between the tuned permeability and diffusion. The diffusion measurements also correlate with the thermodynamic parameters obtained using ITC, a suggestive result that may implicate a reduced level of binding interaction between CA2HE-capped NPs and mucin.

#### ASSOCIATED CONTENT

## Supporting Information

The Supporting Information is available free of charge at https://pubs.acs.org/doi/10.1021/acsanm.3c03807.

NMR characterizations of all six carbon-chained ILs used, percent yields and water contents of all ILs, bare and CA2HE 1:1 PLGA diffusion in water, mucus, and mucin, bare and CA2HE 1:1 PLGA diffusion time study in mucus, and CD concentration study for CA2HE 1:1 PEG—PLGA in PGM (PDF)

## AUTHOR INFORMATION

## **Corresponding Author**

Eden E. L. Tanner — Department of Chemistry and Biochemistry, The University of Mississippi, Oxford, Mississippi 38677, United States; Phone: 662-915-1165; Email: eetanner@olemiss.edu

#### **Authors**

Mary E. VanLandingham – Department of Chemistry and Biochemistry, The University of Mississippi, Oxford, Mississippi 38677, United States; orcid.org/0000-0002-9976-3555

Rebekah A. Heintz – Department of Chemistry and Biochemistry, The University of Mississippi, Oxford, Mississippi 38677, United States

Chathuri S. Kariyawasam – Department of Chemistry, Mississippi State University, Starkville, Mississippi 39762, United States

Donovan S. Darlington – Department of Chemistry and Biochemistry, The University of Mississippi, Oxford, Mississippi 38677, United States

Claylee M. Chism – Department of Chemistry and Biochemistry, The University of Mississippi, Oxford, Mississippi 38677, United States

Sara X. Edgecomb – Department of Chemistry and Biochemistry, The University of Mississippi, Oxford, Mississippi 38677, United States

- Angela Roberts Department of Chemistry and Biochemistry, The University of Mississippi, Oxford, Mississippi 38677, United States
- Jorden Marzette Department of Chemistry and Biochemistry, The University of Mississippi, Oxford, Mississippi 38677, United States
- Nicholas C. Fitzkee Department of Chemistry, Mississippi State University, Starkville, Mississippi 39762, United States; orcid.org/0000-0002-8993-2140

Complete contact information is available at: https://pubs.acs.org/10.1021/acsanm.3c03807

#### Notes

The authors declare no competing financial interest.

## ACKNOWLEDGMENTS

E.E.L.T. acknowledges the College of Liberal Arts and the National Science Foundation (CHE-1757888) for funding. The authors acknowledge R. C. Fortenberry and A. M. Wallace for assistance with the python code. This work was supported in part by the National Institute of Allergy and Infectious Diseases of the National Institutes of Health under Grant R01AI139479 and the National Science Foundation under Grant MCB 1818090 (to N.C.F.). The content is solely the responsibility of the authors and does not necessarily represent the official views of the National Institutes of Health or the National Science Foundation.

### REFERENCES

- (1) Hu, S.; Yang, Z.; Wang, S.; Wang, L.; He, Q.; Tang, H.; Ji, P.; Chen, T. Zwitterionic Polydopamine Modified Nanoparticles as an Efficient Nanoplatform to Overcome Both the Mucus and Epithelial Barriers. *Chem. Eng. J.* **2022**, 428, 132107.
- (2) Lock, J. Y.; Carlson, T. L.; Carrier, R. L. Mucus Models to Evaluate the Diffusion of Drugs and Particles. *Adv. Drug Delivery Rev.* **2018**, *124*, 34–49.
- (3) Leal, J.; Smyth, H. D. C.; Ghosh, D. Physicochemical Properties of Mucus and Their Impact on Transmucosal Drug Delivery. *Int. J. Pharm.* **2017**, *532*, *555*–*572*.
- (4) Illum, L. Nasal Drug Delivery Possibilities, Problems and Solutions. J. Controlled Release 2003, 87, 187–198.
- (5) Barbi, M. d. S.; Carvalho, F. C.; Kiill, C. P.; Da Silva Barud, H.; Santagneli, S. H.; Ribeiro, S. J. L.; Gremião, M. P. D. Preparation and Characterization of Chitosan Nanoparticles for Zidovudine Nasal Delivery. *J. Nanosci. Nanotechnol.* **2015**, *15* (1), 865–874.
- (6) Barz, B.; Turner, B. S.; Bansil, R.; Urbanc, B. Folding of Pig Gastric Mucin Non-Glycosylated Domains: A Discrete Molecular Dynamics Study. *J. Biol. Phys.* **2012**, *38* (4), 681–703.
- (7) Chatzitaki, A. T.; Jesus, S.; Karavasili, C.; Andreadis, D.; Fatouros, D. G.; Borges, O. Chitosan-Coated PLGA Nanoparticles for the Nasal Delivery of Ropinirole Hydrochloride: In Vitro and Ex Vivo Evaluation of Efficacy and Safety. *Int. J. Pharm.* **2020**, *589*, 119776.
- (8) Pornpitchanarong, C.; Rojanarata, T.; Opanasopit, P.; Ngawhirunpat, T.; Bradley, M.; Patrojanasophon, P. Maleimide-Functionalized Carboxymethyl Cellulose: A Novel Mucoadhesive Polymer for Transmucosal Drug Delivery. *Carbohydr. Polym.* 2022, 288, 119368.
- (9) Dedinaite, A.; Lundin, M.; Macakova, L.; Auletta, T. Mucin-Chitosan Complexes at the Solid-Liquid Interface: Multilayer Formation and Stability in Surfactant Solutions. *Langmuir* **2005**, *21* (21), 9502–9509.
- (10) Deacon, M. P.; Mcgurk, S.; Roberts, C. J.; Williams, P. M.; Tendler, S. J. B.; Davies, M. C.; Davis, S. S.; Harding, S. E. Atomic Force Microscopy of Gastric Mucin and Chitosan Mucoadhesive Systems. *Biochem. J.* **2000**, *348*, 557.

I

- (11) Gao, X.; Xiong, Y.; Chen, H.; Gao, X.; Dai, J.; Zhang, Y.; Zou, W.; Gao, Y.; Jiang, Z.; Han, B. Mucus Adhesion vs Mucus Penetration? Screening Nanomaterials for Nasal Inhalation by MD Simulation. *J. Controlled Release* **2023**, *353*, 366–379.
- (12) Mun, E. A.; Hannell, C.; Rogers, S. E.; Hole, P.; Williams, A. C.; Khutoryanskiy, V. V. On the Role of Specific Interactions in the Diffusion of Nanoparticles in Aqueous Polymer Solutions. *Langmuir* **2014**, *30* (1), 308–317.
- (13) Peng, K.; Gao, Y.; Angsantikul, P.; LaBarbiera, A.; Goetz, M.; Curreri, A. M.; Rodrigues, D.; Tanner, E. E. L.; Mitragotri, S. Modulation of Gastrointestinal Mucus Properties with Ionic Liquids for Drug Delivery. *Adv. Healthc. Mater.* **2021**, *10* (13). DOI: 10.1002/adhm.202002192.
- (14) Keller, S.; Vargas, C.; Zhao, H.; Piszczek, G.; Brautigam, C. A.; Schuck, P. High-Precision Isothermal Titration Calorimetry with Automated Peak-Shape Analysis. *Anal. Chem.* **2012**, *84* (11), 5066–5073
- (15) Scheuermann, T. H.; Brautigam, C. A. High-Precision, Automated Integration of Multiple Isothermal Titration Calorimetric Thermograms: New Features of NITPIC. *Methods* **2015**, *76*, 87–98. (16) Le, V. H.; Buscaglia, R.; Chaires, J. B.; Lewis, E. A. Modeling Complex Equilibria in Isothermal Titration Calorimetry Experiments: Thermodynamic Parameters Estimation for a Three-Binding-Site Model. *Anal. Biochem.* **2013**, 434 (2), 233–241.
- (17) Roberton, A. M.; Mantle, M.; Fahim, R. E. F.; Specian, R. D.; Bennick, A.; Kawagishi, S.; Sherman, P.; Forstner, J. F. The Putative 'Link' Glycopeptide Associated with Mucus Glycoproteins. Composition and Properties of Preparations from the Gastrointestinal Tracts of Several Mammals. Biochemical Journal 1989, 261 (2), 637–647.